

11

UPPER ATMOSPHERIC RESEARCH SATELLITE (UARS)  
ONBOARD ATTITUDE DETERMINATION USING A KALMAN  
FILTER

by

Joseph Garrick  
Code 554/Flight Dynamics Analysis Branch  
NASA - Goddard Space Flight Center  
Greenbelt, Maryland

ABSTRACT

The Upper Atmospheric Research Satellite (UARS) requires a highly accurate knowledge of its attitude to accomplish its mission. Propagation of the attitude state using gyro measurements is not sufficient to meet the accuracy requirements, and must be supplemented by an observer/compensation process to correct for dynamics and observation anomalies. The process of amending the attitude state utilizes a well known method, the discrete Kalman Filter.

This study will be a sensitivity analysis of the discrete Kalman Filter as implemented in the UARS Onboard Computer (OBC). The stability of the Kalman Filter used in the normal on-orbit control mode within the OBC, will be investigated for the effects of corrupted observations and nonlinear errors. Also a statistical analysis on the residuals of the Kalman Filter will be performed. These analysis will be based on simulations using the UARS Dynamics Simulator (UARDSIM) and compared against attitude requirements as defined by General Electric (GE). An independent verification of expected accuracies will performed using the Attitude Determination Error Analysis System (ADEAS).

1.0 Introduction

The Upper Atmosphere Research Satellite (UARS) is a three axis stabilized spacecraft, designed to make a global, continuous and comprehensive look at the Earth's upper atmosphere. The spacecraft was launched on September 12, 1991 onboard Space Transportation System 48 (STS-48) and placed in a circular, low earth orbit before ascending to its final mission orbit with mean altitude of 585 km. and inclination of 57 degrees. The mission lifetime will cover two northern hemisphere winters and have a nominal life expectancy of 18 months, with possible extensions up to 15 years.

The UARS observatory consists of ten science instruments, an instrument module (IM) including mission-unique hardware, and the Multimission Modular Spacecraft (MMS). The MMS will provide

precision pointing for the science instruments on an Earth-oriented platform, with periodic routine maneuvers to maintain a favorable sun orientation. The MMS is an on-orbit serviceable spacecraft bus that has a modular design to allow for use on most science related satellites. The observatory uses the MMS to provide attitude control, communications and data handling, electrical power storage and regulation, and propulsion.

Of interest to this study is the MMS Modular Attitude Control Subsystem (MACS) which provides the Attitude Determination and Control (AD&C) subsystem software that is implemented in the Onboard Computer (OBC), which is part of the Command and Data Handling (C&DH) subsystem. The OBC provides the estimation model for meeting the attitude determination accuracy during the precision mode of the normal on-orbit mission mode of 60 arcsec. (3 sigma). An important part of the attitude determination scheme implemented in the OBC is to compensate the propagated state using gyro data with periodic measurement data from the Fixed Head Star Trackers (FHSTs) to obtain a better estimate of the current attitude error and gyro drift bias. This compensator is known as the discrete Kalman Filter. This study will address the attitude determination capabilities of the discrete Kalman Filter during the precision pointing mode of the normal on-orbit mission as implemented in the OBC of the UARS spacecraft.

2.0 Attitude Modeling

This study will be a sensitivity analysis of the discrete Kalman Filter as implemented in the UARS spacecraft. The stability of the Kalman Filter will be investigated for the effects of corrupted observations and nonlinear errors. Also a statistical analysis on the residuals of the Kalman Filter will be performed. These analysis will be based on simulations using the UARS Dynamics Simulator (UARDS), a software implementation of the spacecraft's hardware and control systems. An independent verification of expected accuracies will also be performed using the Attitude Determination Error Analysis System (ADEAS).

2.1 Attitude Determination Error Analysis System (ADEAS)

One of the attitude tools used in this study was the Attitude Determination Error Analysis System (ADEAS), which allowed for a quick verification of expected accuracies. ADEAS can model estimation by using either a batch filter or a Kalman Filter. The estimation choices found in ADEAS makes this tool ideal for comparison against simulation results using the UARDS and the definitive attitude ground solutions using a batch filter. The means by which ADEAS computes the attitude accuracies is the solve-for and consider parameters supplied by the user. The solve-for parameter are those found in the UARS state vector. In the UARS case these are the attitude errors and the gyro drift errors. The consider parameters are those not found in the state vector of the OBC and not taken into account by the filter, such as misalignments.

## 2.2 UARS Dynamics Simulator (UARSDS)

The UARS Dynamics Simulator (UARSDS) is an analytical tool developed to give the analysts an insight into the performance of the attitude determination and control system used onboard the spacecraft. By means of interactive screen displays the user can configure the UARS spacecraft to include misalignments, noises, biases and scale factors to all of the modeled hardware. The dynamics can be configured to include initial attitude and rate errors, as well as the ability to include or exclude the effects due to external perturbations, such as environmental torques and cryogenic venting. Also, the user can specify the desired orbital characteristics for a given epoch to allow the choice of seasonal variations of sun and moon viewing data, as well as continually changing star and target position vectors. A simulation using the UARSDS is controlled using the same set of ground commands used by the actual spacecraft, thus allowing the simulator to create a realistic scenario actually employed during the spacecraft's mission.

## 2.3 UARS Attitude Determination

The UARS onboard attitude determination function is contained in two parts within the OBC. The first part contains the routines which propagate the state vector using gyro data and compensates the state vector during the normal on-orbit modes every 32.768 seconds (64 OBC cycles) using the results from the second part, the attitude estimation function. The attitude estimation function contains the discrete extended Kalman Filter and is processed every 64 OBC cycles to produce update parameters. The following sections give a more detailed mathematical view of the attitude determination process.

### 2.3.1 Kinematic Equations (Time Propagation)

This process updates the spacecraft Euler parameters using the angular increments furnished by the gyro data processor. When the update filter (the Kalman Filter) processing is enabled, the Euler parameters are also compensated using update parameters from the attitude estimation function. Also the gyro biases, which are used in the gyro data processor, are corrected. The equations for propagating and compensating the OBC state vector are as follows:

1. Compute the Euler parameter updates

$$\delta Q = \frac{1}{2} \Omega(\theta) Q \quad (2-1)$$

$$\text{where } \Omega(\theta) = \begin{bmatrix} 0 & \theta_z & -\theta_y & \theta_x \\ -\theta_z & 0 & \theta_x & \theta_y \\ \theta_y & -\theta_x & 0 & \theta_z \\ -\theta_x & -\theta_y & -\theta_z & 0 \end{bmatrix}$$

$\theta_{x,y,z}$  are gyro compensated data

$$Q = [q_1, q_2, q_3, q_4]^T$$

2. Update the Euler parameters

$$Q_{t+1} = Q_t + \delta Q \quad (2-2)$$

3. Normalize the update Euler parameters

$$Q_{t+1} = Q_{t+1} * Q^{-1} \quad (2-3)$$

$$\text{where } Q^{-1} = 1 + \frac{1}{2} (1 - |Q_{t+1}|^2)$$

4. If update filter processing is enabled update the attitude and gyro biases.

- a. Compute the Euler parameter updates

$$\delta Q' = \frac{1}{2} \Omega(\delta\theta) Q_{t+1} \quad (2-4)$$

$$\text{where } \delta\theta = S_i \quad i = 1, 2, 3$$

$S = [s_1, s_2, s_3, s_4, s_5, s_6]$   
and is the update parameters from the attitude estimation function

- b. update the Euler parameters

$$Q_{t+1} = Q_{t+1} + \delta Q' \quad (2-5)$$

- c. update the gyro biases

$$b_i = b_i + (S_{i,3} * t_c) \quad i = 1, 2, 3 \quad (2-6)$$

where  $b_i$  are gyro biases

$t_c$  is the OBC cycle time  
(0.512 sec.)

### 2.3.2 Discrete Kalman Filter

The discrete Kalman Filter has three processing steps. The first is the computation of the state transition matrix, the state noise covariance matrix, and the state covariance matrix. The state transition matrix and the state noise covariance matrices are computed once and recomputed only if the measurement update interval changes. The second step is the measurement model. The measurement model uses two Fixed Head Star Trackers (FHST) as the source of measurement data for nominal processing. In the event one of the FHSTs degrade in performance, then a Fine Sun Sensor (FSS) replaces the failed FHST as the source of data. FHST data is compared against a list of OBC guide stars to find a match based on magnitude and position thresholds, to produce an estimate of position error. The FSS makes use of an onboard ephemeris generator for the 'true' Sun position in its computation of a position error. The output of the measurement model is the Kalman gains used to compensate the state vector, which contains a representation of the attitude error and the gyro biases. Finally, the third step uses the Kalman gain and measurement matrices from the second step to propagate the state covariance matrix, to be used during the next measurement update.

### 2.3.2.1 Dynamics Model

The state transition and state noise covariance matrices are obtained from the dynamics model. The derivation of the dynamics model and thus the matrices are presented in the following paragraphs. First, the gyro rates are described as

$$\dot{\theta} = \dot{w} - b_0 - b + n_v \quad (2-7)$$

$$\dot{b} = n_u \quad (2-8)$$

where  $\dot{\theta} = [\dot{\theta}_x, \dot{\theta}_y, \dot{\theta}_z]$  is gyro rate measurements

$\dot{w} = [w_x, w_y, w_z]$  is true spacecraft body rates

$b_0 = [b_{0x}, b_{0y}, b_{0z}]$  is gyro bias

$b = [b_x, b_y, b_z]$  is gyro drift bias

$n_v = [n_{vx}, n_{vy}, n_{vz}]$  is float torque noise (Gaussian white noise)

$n_u = [n_{ux}, n_{uy}, n_{uz}]$  is float torque derivative noise (Gaussian white noise)

The attitude rate error is defined as follows:

$$\alpha = \dot{\theta} - \dot{w} = -b_0 - b + n_v \quad (2-9)$$

The gyro bias is assumed to be known and therefore it can be removed from equation 2-9, leaving the following:

$$\alpha = -b + n_v \quad (2-10)$$

The two equations, 2-8 and 2-10, then give the dynamics model. It can be written in the form

$$\dot{X}(t) = [A] X(t) + W(t) \quad (2-11)$$

where  $X(t) = [\alpha, b]^T$  is the state vector

$$W(t) = [n_{v_i}, n_{u_i}]^T \quad i = 1, 2, 3$$

$$[A] = \begin{bmatrix} w_{3 \times 3} & : & -I_{3 \times 3} \\ \dots & & \dots \\ 0_{3 \times 3} & : & 0_{3 \times 3} \end{bmatrix}$$

The discrete state transition matrix is derived from [A] and is given by

$$\Phi_T = e^{[A]T} \quad (2-12)$$

Where T is the measurement update interval. This expression can be approximated by a Taylor's expansion as

$$\Phi_T = I + [A]T + 1/2([A]T)^2 + 1/6([A]T)^3$$

$$\Phi_T = \Phi(t_k, t_{k-1})$$

$$T = t_k - t_{k-1}$$

Knowing the state transition matrix we can now

solve for the noise covariance matrix, [W].

$$W_T = \int_{t_{k-1}}^{t_k} \Phi(t_k, \tau) Q(\tau) \Phi^T(t_k, \tau) d\tau \quad (2-13)$$

Where  $Q(t) = E[W(t) W^T(t)]$  and is known as the spectral density matrix. The evaluation of  $Q(t)$  is

$$Q(t) = \begin{bmatrix} n_v n_v^T & : & 0_{3 \times 3} \\ \dots & & \dots \\ 0_{3 \times 3} & : & n_u n_u^T \end{bmatrix}$$

The resulting matrix is a main diagonal matrix since the following characteristics hold

$$E[n_{v_i} n_{v_j}] = 0 \quad \text{for } i \neq j$$

$$E[n_{u_i} n_{u_j}] = 0 \quad \text{for } i \neq j$$

$$E[n_{v_i} n_{u_j}] = 0 \quad \text{for any } i \text{ and } j$$

Now we have everything to propagate the state covariance matrix. The equation for the propagation of the state covariance matrix in the time update step is

$$P_i = \Phi_T P_{i-1}^* \Phi_T^T + W_T \quad (2-14)$$

where  $P_i$  is the a priori propagated state covariance matrix for this update interval

$P_{i-1}^*$  is the a posteriori updated state covariance matrix from previous interval

At initialization the state covariance matrix is a main diagonal matrix given initial values as specified by the ground for the attitude error variances, upper left submatrix, and the gyro bias variances, lower right submatrix. The other submatrices are given the initial value of zero.

### 2.3.2.2 Measurement Model

This process determines whether the update filter state covariance matrix require updates and, if so, which sensor data are used to perform the update. The ground has the ability to select different sensor configurations. In nominal conditions the two FHSTs are used as the source of measurement data. In the event of a degraded FHST then an FSS can be selected by the ground to replace the failed sensor. Data is used from only one of the sensor pair at each update interval, and is the sensor that has gone the longest time period without providing update data. This is nominally an alternating scheme between the sensor pair with targets visible in each field of view (FOV). The measurements from the sensor is compared against known 'true' data provided by the OBC system tables, for guide stars, or an ephemeris generation routine, for sun data. Once valid data is found, position errors are generated, which are used to generate the update state vector used in the kinematic equations and to generate measurement matrices used in the Kalman Filter update routines.

The algorithms for the measurement model are as follows:

1. Compute the residuals

$$Z(i) = OS(i) - CS(i) \quad i = x, y \quad (2-15)$$

where OS is the observed target vector in the sensor coordinate frame created from sensor measurement data

CS is the computed target vector in the sensor coordinate frame created from OBC 'true' data

2. Form the measurement matrix

The measurement model is given by the equation

$$Z_k = H_k X_k + R_k$$

where  $Z_k$  is a measurement at time  $k$   
 $H_k$  is transformation matrix  
 $R_k$  is Gaussian white noise

$$H_k = \begin{bmatrix} (X \times S_k)^T : 0_{1 \times 3} \\ \dots \dots \dots \\ (Y \times S_k)^T : 0_{1 \times 3} \end{bmatrix}$$

where  $S_k$  is observed target vector in the spacecraft body frame

$X, Y$  are the reference vectors and are defined as follows:

FHST:  $X$  and  $Y$  are just the x-axis and the y-axis unit vectors of the FHST in the spacecraft body frame

FSS:  $X$  and  $Y$  are defined as

$$X_i = (X_{Fi} - XE * Z_{Fi}) / S_k(z) \quad i = x, y, z$$

$$Y_i = (Y_{Fi} - YE * Z_{Fi}) / S_k(z) \quad i = x, y, z$$

where  $X_f$  is the FSS x-axis in the spacecraft frame

$Y_f$  is the FSS y-axis in the spacecraft frame

$Z_f$  is the FSS z-axis in the spacecraft frame

$XE, YE$  are the FSS 'true' x and y axis vectors computed from sun vector in FSS coordinates

3. Form the measurement error variance matrix

$$R = \begin{bmatrix} R_1 & 0 \\ 0 & R_2 \end{bmatrix} \quad (2-16)$$

$$R_k = E[V_k V_k^T]$$

where  $V_k$  is the sensor noise (Gaussian)

2.3.2.3 Update Algorithms (Measurement Update)

The final step in the Kalman Filter is to update the state covariance matrix and compute the state vector update parameters used in the kinematic equations. The algorithms in matrix form for the update are

1. Gain matrix computation (2-17)

$$K_k = P_k - H_k^T (H_k P_k - H_k^T + R_k)^{-1}$$

2. Gyro Bias and Euler parameter correction (2-18)

$$X_k^* = X_k + K_k (Z_k - H_k X_k)$$

3. State covariance matrix update (2-19)

$$P_k^* = P_k - K_k H_k P_k$$

In the UARS OBC the algorithms are processed in a sequential manner, thus changing it to a scalar implementation and requiring a two pass system to process both measurement vectors. Equation 2-18 is actually implemented in the kinematic equations, with the state update vector computed in the measurement model. It is easier to follow the scalar two pass implementation by first noting the following

$$P_k = \begin{bmatrix} P_{11} : P_{12} \\ \dots \dots \dots \\ P_{21} : P_{22} \end{bmatrix}$$

$$K_k = [K_1 \dots \dots K_6]$$

Pass One:

$$H = [(X \times S_k)^T : 0_{1 \times 3}]$$

$$K_k = P_{12} H^T / (H P_{11} H^T + R_1)$$

$$S = Z_1 K_k$$

$$P_k = P_k - K_k H P_k$$

Pass Two:

$$H = [(Y \times S_k)^T : 0_{1 \times 3}]$$

$$K_k = P_{12} H^T / (H P_{11} H^T + R_2)$$

$$S = S + (Z_2 - H S) K_k$$

$$P_k^* = P_k - K_k H P_k$$

2.4 Sensor Models and Coordinate Systems

The next few sections will give a brief description of the sensor models and their coordinate systems as modeled by the UARS Dynamics Simulator.

Detailed descriptions of the models can be found in reference 1.

#### 2.4.1 Fixed Head Star Tracker (FHST)

The FHST is an attitude sensor that searches for, detects, and tracks stars; provides accurate position and intensity information for stars in its field of view (FOV); and generates status flags and parameters characterizing the sensor operation. The position of the star is output as a horizontal (H) and vertical (V) coordinate pair, with the H and V axis describing the projection onto a plane perpendicular to the camera boresight.

The nominal coordinate system of the FHST is defined by a series of rotations from the spacecraft body coordinate system (BCS) to the FHST coordinate system (FCS). The transformation is a 3-2-3 Euler sequence:

$$M_{FB} = M_3(\theta_1) M_2(\theta_2) M_3(\theta_3)$$

where for FHST 1;

$$\theta_1 = 51.9 \text{ deg.}, \theta_2 = 105.6 \text{ deg.}, \theta_3 = 0 \text{ deg.}$$

and for FHST 2;

$$\theta_1 = 128.1 \text{ deg.}, \theta_2 = 105.6 \text{ deg.}, \theta_3 = 0 \text{ deg.}$$

The subscript FB denotes a transformation from BCS to FCS.

#### 2.4.2 Fine Sun Sensor (FSS)

The FSS is an attitude sensor that provides two-axis Sun direction information with respect to the sensor axis. Output consists of angles between the boresight and the sun vector, which are projected into a plane described by a vertical axis (beta) and the horizontal axis (alpha).

The nominal FSS coordinate system is defined by a 3-2-3 Euler rotation:

$$M_{SB} = M_3(\theta_1) M_2(\theta_2) M_3(\theta_3)$$

where the rotations are

$$\theta_1 = 33.1 \text{ deg.}, \theta_2 = -100.5 \text{ deg.}, \theta_3 = 0 \text{ deg.}$$

The subscript SB denotes a transformation from BCS to sun sensor coordinate system (SCS).

#### 2.4.3 Inertial Reference Unit (IRU)

The IRU is an attitude rate sensor consisting of a gyro package that measures inertial vehicle rates about the sensor axis. The output of the IRU consists of analog rates, accumulated angles, range status and temperature.

The nominal IRU coordinate system is defined as being coincident with the spacecraft body axis coordinate system. Equation 2-7 describes each gyro output, where  $w$  in the equation is the

measured body rate for that gyro.

### 3.0 Onboard Attitude Accuracy

As stated earlier, UARS requires a highly accurate knowledge of its attitude to allow the instruments on board to perform precise measurements of the earth's atmosphere. The attitude determination requirement placed on the OBC during the normal mission phase is 60 arcsec. (3 sigma) per axis using two FHSTs and 70 arcsec. (3 sigma) using one FHST. The requirements for attitude determination were generated by G.E. using prelaunch sensor alignments, which accounts for the overwhelming majority of the attitude determination uncertainties. The prelaunch alignment uncertainties for the FHST and FSS sensors are

Sensor	Prelaunch Alignment Uncertainty (arcsec, 3 sigma)		
	Roll	Pitch	Yaw
FHST 1	55.3	55.3	55.2
FHST 2	55.3	55.3	55.2
FSS	200.0	200.0	200.0

A study was done by Flight Dynamics to determine the expected on-orbit attitude uncertainties after sensor calibration. The first step in this process was to determine the expected on-orbit sensor alignment accuracies after calibration. The procedure for this analysis is given in reference 2, with the results of this analysis given as

Sensor	Postlaunch Alignment Uncertainty (arcsec, 3 sigma)		
	Roll	Pitch	Yaw
FHST 1	39	47	49
FHST 2	40	48	48
FSS	63	65	44

Using these calculated on-orbit sensor alignment uncertainties, the on-orbit attitude uncertainties were determined using ADEAS. Because UARS is a momentum biased system with a one rotation per orbit about the pitch axis, a few different scenarios arises with target availability for the sensors. With the two FHST configuration, most of the time there is an abundance of target opportunities per orbit. However, during certain times of the year the availability of guides stars drops to around only five per orbit. With one FHST and one FSS to replace the failed FHST, not only is guide stars of concern, but also the amount of time the Sun is in the FSS FOV. Nominally the Sun is in the FOV for about twenty minutes out of the orbit, but there will be times when the FSS will not see the sun for the entire orbit. The attitude accuracies were determined for these scenarios using ADEAS with expected alignment uncertainties, and measurement and dynamics noise values. The results are given as

C-7

Sensor	Post-calibration Attitude Uncertainty (arcsec., 3 sigma)			RSS
	Roll	Pitch	Yaw	
Two FHSTs (star rich)	41	55	32	76
Two FHSTs (star poor)	43	62	32	82
FHST/FSS (star rich)	53	60	41	90
FHST/FSS (star poor)	55	63	44	95
One FHST (star rich)	56	63	43	95
One FHST (star poor)	58	70	44	100

Based upon this prelaunch analysis, the attitude determination function should be able to meet the requirements set up by the project office after calibration of the sensor alignments. It's interesting to note that FSS data does not seem to affect the attitude accuracy significantly when comparing the FHST/FSS and the one FHST configurations for both star rich and star poor orbits.

Comparisons of typical OBC and ground attitude solutions over an orbit for the two FHST configuration after calibration are given below

	3 Sigma (arcsec.)			
	Roll	Pitch	Yaw	RSS
UARS OBC star rich	5.1	28.2	7.2	29.5
UARS OBC star poor	12.6	31.9	13.2	36.8

The attitude solution shows a dramatic improvement over what was expected. To compare actual results and ADEAS results with the dynamics simulator and establish some bounds for expected performance of the OBC, two simulations were made, one with perfect knowledge of alignments and noises by the OBC, and another using anticipated post-calibration alignments with perfect knowledge of noise for a star rich orbit. The results are

	3 Sigma (arcsec.)			
	Roll	Pitch	Yaw	RSS
Dyn. Sim (perfect)	1.0	21.2	1.2	21.3
Dyn. Sim (expected)	25.0	33.8	24.4	48.6

In comparing the dynamics simulator runs with the actual results of a star rich orbit, similar results are given verifying the dynamics simulator as a reasonably accurate tool for this analysis. The results also made clear that the post-calibration alignment uncertainties were better than expected. Similar runs were made for the FHST/FSS sensor configuration as for the two FHST configuration, with the following results.

	3 Sigma (arcsec.)			
	Roll	Pitch	Yaw	RSS
FHST/FSS (perfect)	4.9	31.4	3.3	31.9
FHST/FSS (expected)	31.2	61.0	23.7	72.5

The dynamics simulator case with the expected

post-calibration alignments are comparable with the ADEAS results. Then depending on the actual alignment uncertainties the results should fall somewhere in between these two bounds. This also is a good illustration of how the alignment uncertainties dominate the attitude determination accuracy. One final simulation was made using only one FHST in a star rich orbit with perfect alignment and expected noise.

	3 Sigma (arcsec.)			
	Roll	Pitch	Yaw	RSS
One FHST (perfect)	11.9	41.1	2.4	42.9

Notice how little improvement is made by adding the FSS along with a FHST. This is due to the availability of an abundance of star measurements, while the FSS approximately has the Sun in the FOV for at most twenty minutes of each orbit.

#### 4.0 Sensitivity Analysis

This sensitivity analysis is designed to determine the responses of the attitude determination function (which includes the Kalman Filter) due to noise and modeling errors, via analysis of simulations using the dynamics simulator by varying parameters. To keep this paper within a respectable length, only the sensor configurations for a star rich orbit will be considered. The study will look at the attitude determination accuracy, steady state values and measurement residual statistics as a result of varying alignment and modeling errors. The results are given in tabular and graphical form, whichever is most informative. The graphical representations will include a polynomial fit to show any trends for possible predictions.

#### 4.1 Misalignment of Sensors

The affect of misaligning the sensors is to create an offset from the normal pointing, around which the sensors will try to null out measurement errors. This change in attitude pointing will necessitate a compensation of the measured body rates in the OBC for any movement of the boresights within or out of the plane that is described by the two sensor boresights. The misalignments were applied to both of the FHST sensors, such as not to separate the boresights in or out of the plane. Figure 1 shows what the OBC determines its attitude to be as a result of increasing misalignments about each of the FHSTs axis. Figure 2 gives the actual attitude determination error from the known truth.

Comparison of the two plots shows that the misalignments are not observable in the attitude, as expected. Notice also, that the attitude is insensitive to small rotations about the boresight, because of this rotation is about the body pitch axis and is interpreted as an insignificant pitch rate bias. The residuals did not show any increase in variance (lack of observability of boresight reorientation and rotations about the boresight), but the gyro biases increased due to the reorientation of the spacecraft's attitude pointing.

Attitude Determination Accuracy RSS  
for FHST misalignment each axis  
(Kalman Filter viewpoint)

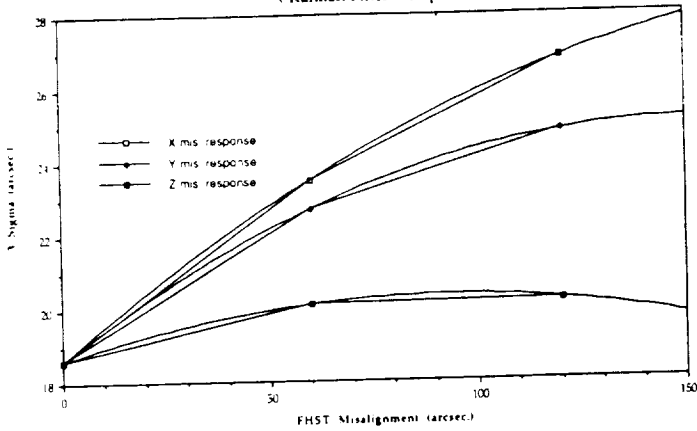


Figure 1

Attitude Determination Accuracy RSS  
for FHST misalignment each axis  
(Actual attitude accuracy)

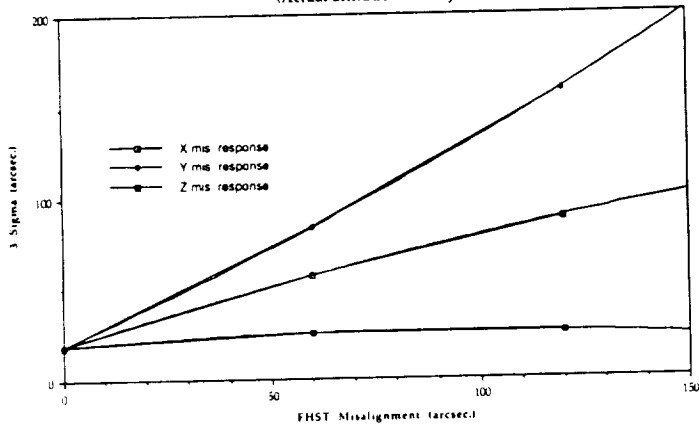


Figure 2

The gyro bias needed to compensate for each of the misalignments are given for each axis in Figures 3, 4 and 5.

Gyro Bias Response to FHST  
Misalignment of X axis

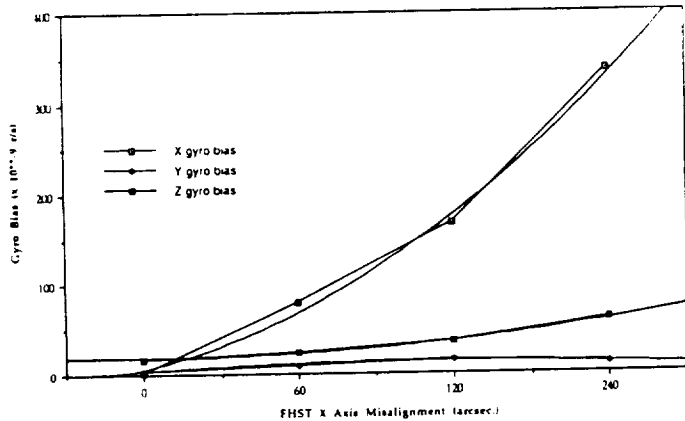


Figure 3

Gyro Bias Response to FHST  
Misalignment of Y Axis

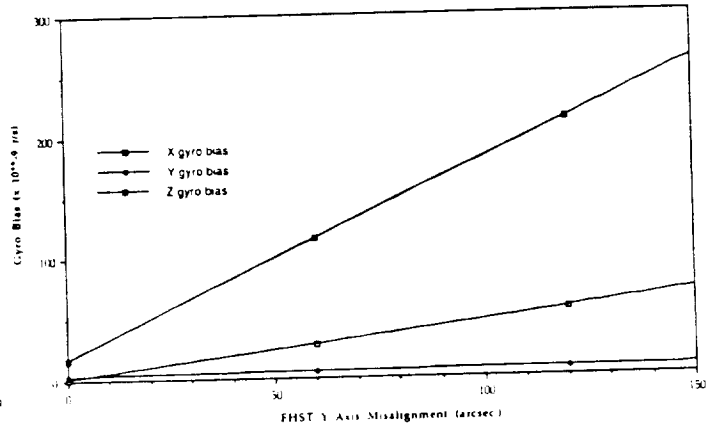


Figure 4

Gyro Bias Response to FHST  
Misalignment of Z Axis

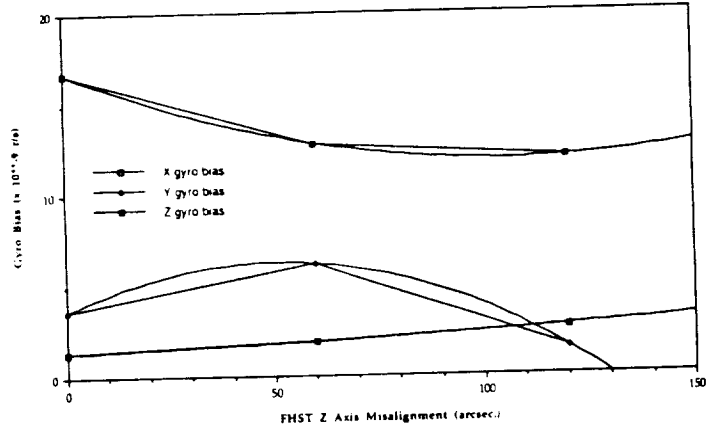


Figure 5

The y-axis (pitch axis) shows no change in gyro bias for any of the rotations. This is because the bias is very small as compared to the pitch rate, and therefore indistinguishable. Attitude determination accuracy was more sensitive to misalignments about the FHST x-axis, which is also reflected in the gyro bias results. Of interest would be how much misalignment would be tolerated before a particular axis exceeds the 60 arcsecond (3 sigma) requirement. The prediction is obtained from the polynomial fit to the data and are estimated to in the following table. The dominate axis is the one most sensitive to the disturbance and first exceeds the requirement.

FHST Alignment Tolerance (arcsec., 3 sigma)			
	X-axis	Y-axis	Z-axis
Misalignment (arcsec.)	54	39	None
Dominate Axis	Z	X	--

The comparison of the attitude determination accuracy for the misalignment of the FSS are given in figures 6 and 7. In these simulations only the FSS was misaligned about each of its axis.

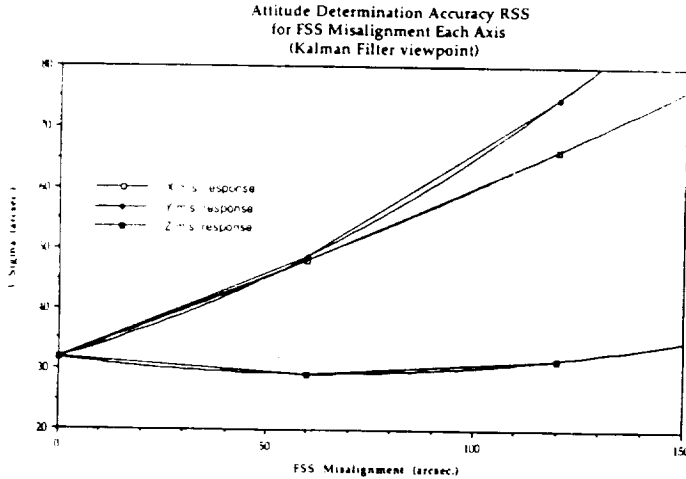


Figure 6

Again, it is seen that the OBC has no accurate knowledge in the attitude for movement of the boresights relative to each other (nor would there be any notice in the residuals or gyro bias for any common movement to each other).

However, the Kalman Filter this time reflects some change in attitude.

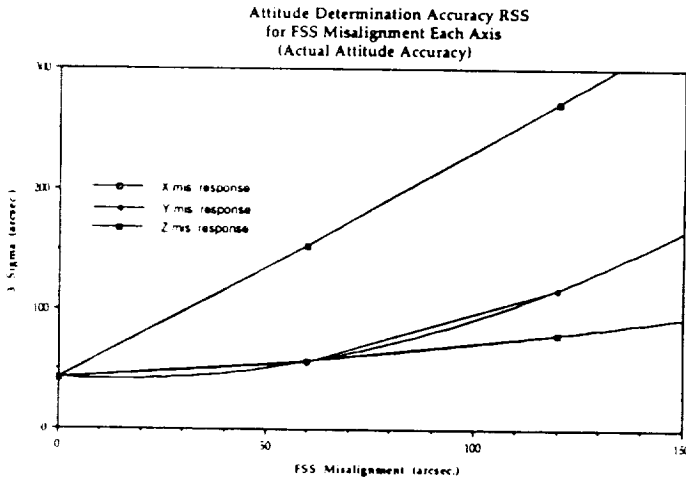


Figure 7

This is because there is some separation between the two boresights, which in turn produces residuals each time sensors are toggled for data. The variance of the residuals are given by

FSS Misalignment Residual  
Variances (arcsec\*\*2)

Rotation (arcsec.)	X-axis		Y-axis		Z-axis	
	z1	z2	z1	z2	z1	z2
0	1069	2845	1069	2845	1069	2845
60	1273	3370	1644	3115	1105	2773
120	1524	4180	3307	3477	1225	2789

This bouncing affect is of course more pronounced as the misalignments increase. The increase in residual variance in turn is observed in the measurement model, which acts to null out the measurement error around the new pointing. It can be seen that the attitude accuracy is sensitive in this case to a misalignment about all axis, including the boresight (because this rotation is mostly about the body roll axis, the x-axis). The z-axis showed no residual response to misalignment. The boresight didn't move with respect to the FHST, and therefore there was no bouncing in switching between sensors. Also the FHST dominated around the orbit with its perfect measurements, compared with only twenty minutes shared between the FHST and FSS when the sun was in the FOV. Figures 8, 9 and 10 show the gyro bias response to the new attitude pointings. It is also seen here that the gyro biases are sensitive to a rotation about the boresight. As with the two FHST case, an estimate of the alignment tolerance before the accuracy exceeds the 70 arcsecond (3 sigma) requirement is

FSS Alignment Tolerance (arcsec.)

	X-axis	Y-axis	Z-axis
Misalignment	16	78	98
Dominate Axis	Y	Y	Y

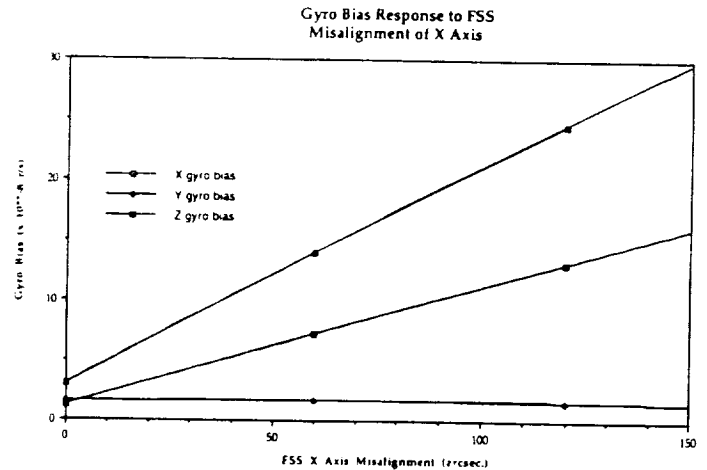


Figure 8

Gyro Bias Response to FSS Misalignment of Y Axis

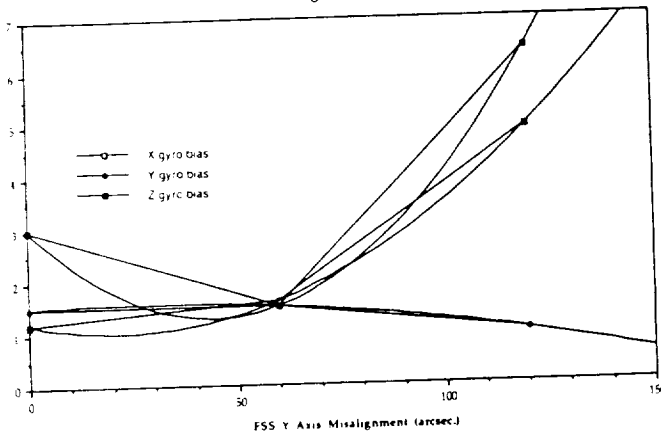


Figure 9

Gyro Bias Response to FSS Misalignment of Z Axis

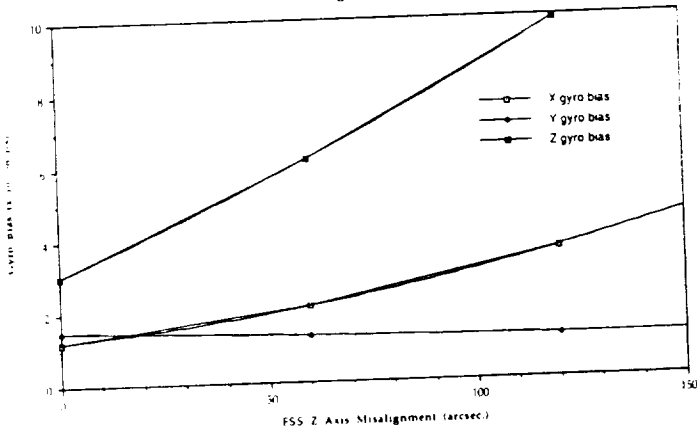


Figure 10

As expected the misalignment of the gyro's has no affect on the measurement residuals and attitude determination accuracy. The OBC compensates for gyro misalignments by solving for gyro biases that maintain the correct pointing. The same holds true for an incorrect modeling in the scale factor that converts the digital information into engineering units. A difference in the scale factor is like introducing a bias to the rate information, and is handled by solving for a OBC gyro bias to compensate.

#### 4.2 Measurement Noise

The attitude determination accuracy response to measurement noise on the FHST and FSS was determined by setting the OBC to have perfect knowledge about alignments and dynamics noise. Thus all changes in response can be attributed to only measurement noise variation. The measurement noise is taken to be Gaussian white noise, with zero mean and increasing variance. The noise is applied to the output measurements. Figure 11 shows the attitude determination accuracy response to noise applied to each of the FHST axis independently.

Attitude Determination Accuracy RSS For FHST Noise Each Axis

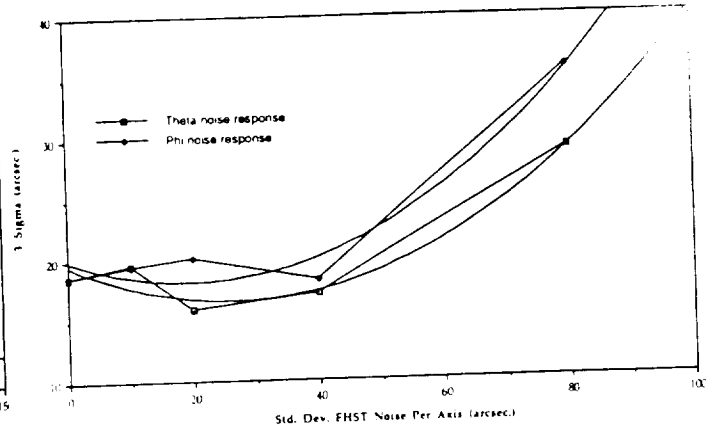


Figure 11

The graph of the two axis show a minimum around 20 to 30 arcseconds. This is where the measurement noise is correctly accounted for by the OBC model, which has lower and upper measurement noise range of 14 and 28 arcseconds, respectively. So this graph shows the affect of the difference of the actual sensor noise from the modeled or expected. As before a prediction is made of when the response will exceed the 60 arcsecond (3 sigma) requirement.

FHST Measurement Noise Tolerance (arcsec.)

	Theta	Phi
Noise (sigma)	126	124
Dominate Axis	Y	Y

The attitude determination accuracy in response to measurement noise on each of the FSS axis is shown in Figure 12.

Attitude Determination Accuracy RSS for FSS Noise Each Axis

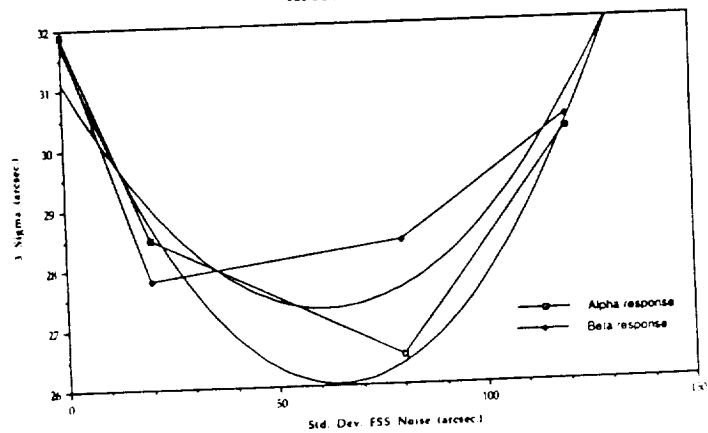


Figure 12

In this case the few data points produces a poor polynomial fit to the data. But like the FHST case, this graph shows the affect of a difference in actual measurement noise and that which is modeled in the OBC. Here, the minimum seems to exist over a larger range of noise. An approximation to this range from this graph seems to be 20 to 80 arcseconds. The OBC model in fact computes the lower and upper measurement noise as a function of the alpha and beta measurements, which produces a range of 24 to 96 arcseconds. An estimate is given for the noise tolerance on the FSS before the attitude determination exceeds the 70 arcseconds (3 sigma), with the note that a larger uncertainty is present do to the poor fit of the data.

FSS Measurement Noise Tolerance (arcsec., 3 sigma)		
Noise (sigma)	Theta	Phi
Dominate Axis	Y	Y

As expected, the increase in measurement noise, increased the residual variance for both the FHST and FSS. An example is given for the worse case, the FSS, in Figure 13.

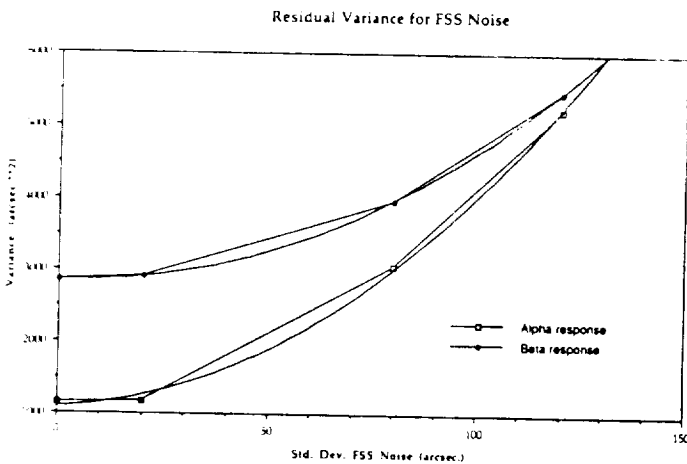


Figure 13

#### 4.3 Dynamic Noise

Equation 2-11 shows that the attitude is affected by both float torque noise (Gaussian white) and float torque derivative noise (also called random walk). The float torque noise produced no significant response to the attitude determination accuracy. The random walk noise, however, showed a large effect in the accuracy. This is because the random walk is integrated over time to produce a gyro drift bias, which at the next measurement time is not estimated accurately by the dynamics model in the Kalman Filter. The float torque noise is a discrete Gaussian random variable that has no correlation with previous or future samples of the noise, and no accumulative affect between measurement updates. Figure 14 show the affect of a random walk noise that is different from the modeled.

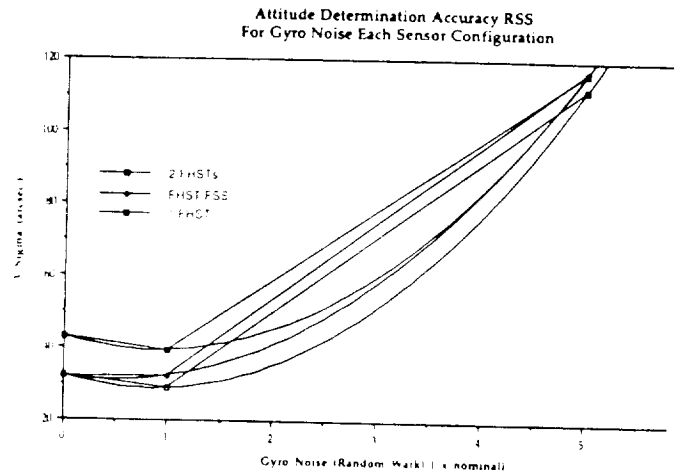


Figure 14

The minimum occurs, as it should, at the gain of one, where the model and actual agree. The random walk noise at this point is approximately  $2.0e-10 \text{ r}/(\text{s}^{**1.5})$  (or approximately  $4.0e-5 \text{ arcsec}/(\text{s}^{**1.5})$ ). The response diverges rapidly as the difference from the modeled increases. The graph also demonstrates that the response is the same for each of the sensor configurations. This is not unexpected, since the noise is applied to the gyro rate measurements and compensated for by estimating a correctional gyro bias in the filter. The estimated tolerance for dynamic noise is

Dynamic Noise Tolerance (gain x nominal)			
Noise (gain)	2 FHST	FHST/FSS	1 FHST
	5.1	4.7	2.7
Dominate Axis	X or Y	Y	Y

#### 5.0 Conclusions

It's been demonstrated with this analysis how the attitude uncertainties is being, and can be met for the three sensor configurations. The FHST alignment uncertainty is currently well within specifications according to the ground attitude solutions, with the jury still out on how well the FSS will perform. With the aid of analysis tools like ADEAS and the dynamics simulator, it can be predicted what to expect for each of these scenarios. The question that needs to be asked now is how important is the need to calibrate the sensors for misalignments and under what circumstances will misalignments not be observable by the Kalman Filter. Also, when will retuning of the Kalman Filter model be necessary and what are the consequences of changing measurement and dynamic noise models.

Looking at the misalignments, the FHST/FSS cases demonstrated the response to separation of the boresights relative to one another. The FSS showed a dramatic sensitivity to rotations about the sensor x-axis, whereas very little influence on attitude determination about the other two axis.

## References

1. T. Sheu Upper Atmosphere research Satellite (UARS) Dynamics Simulator Engineering Model Specifications, Volume 1 and 2, April 1989
2. J. Golder, M. Nicholson, Upper Atmosphere Research Satellite (UARS) Ground Definitive Attitude Determination Error Analysis, January, 1991
3. G.E., Astro Space Division, UARS Critical Design Review Documentation, May 1986
4. G.E., Astro Space Division, Computer Program Design Specification for the Upper Atmosphere Research Satellite (UARS) Flight Software (As-built), April, 1990
5. J. Wertz, Spacecraft Attitude Determination and Control, D. Reidel Publishing Company, 1985

This is surely because the FHST, which was not perturbed, provided accurate measurement data for the body pitch and yaw axis. The rotation about the FSS x-axis, is mostly about the body x and y-axis. It seems that the x-body motion was observable and the gyro bias was computed to compensate for this component of the rotation and the change in attitude pointing about this axis. However, the pitch (body y-axis) motion for any of the three axis rotations, seemed to be absorbed into the large pitch rate without affecting the attitude estimation or gyro bias about this axis. In the two FHST case, where the misalignments of the sensors were the same relative to another, the results show a lack of observability by the Kalman Filter for any of the rotations in the attitude state. The ability to calibrate the alignments of the FHSTs in this case is dependent on the availability of accurate measurements from a third source. Both scenarios shows that the Kalman Filter is at least partially blind to misalignments of the sensors. The process of eliminating these uncertainties, as much as possible, greatly improves the attitude determination error.

The coarser measurement source, the FSS, is able to tolerate more measurement noise than the FHST before the attitude determination shows any divergence and the requirement is exceeded. The OBC measurement model allows the FSS measurements to accommodate a larger tolerance to noise in the data than the FHST, before it begins to affect the attitude state. The consequence though of allowing larger measurement noise is a larger transient to steady state and indeed a different value of steady state do to the increased tolerance to a noisy signal, and therefore larger uncertainty to the true attitude knowledge. The same concern is present in the dynamics with the introduction of a random walk noise. The results of the analysis show the same effect of not properly modeling the drifting gyro measurements. And like the measurement noise, the dynamic noise at some point will cause enough uncertainty in the rate data to warrant an alternative source of rate measurements and/or adjusting filter parameters, with the same consequences.

The choice of preferred sensor configuration is dictated not only by the modeling parameters and filter transient and steady state behavior, but also the availability of stars in the orbit. It was shown in this study that all three configurations would be able to meet requirements with a star rich orbit, and that sun measurements added little to the attitude determination capability. Thus, it might be just as good to use the remaining FHST if one should fail or degrade. It may be desirable if the FSS exhibits large alignment uncertainties or a large noise variance in the signal. When a star poor orbit is encountered, the FSS measurements are sure to be a welcome source for added information to supplement the few FHST measurements, even if it is at most only twenty minutes out of the orbit.

